J Low Temp Phys (2018) 193:258–266
https://doi.org/10.1007/s10909-018-1917-0

Toward Large Field-of-View High-Resolution X-ray Imaging Spectrometers: Microwave Multiplexed Readout of 28 TES Microcalorimeters

W. Yoon[1,2] · J. S. Adams[1,3] · S. R. Bandler[1] · D. Becker[4] · D. A. Bennett[4] · J. A. Chervenak[1] · A. M. Datesman[1,5] · M. E. Eckart[1] · F. M. Finkbeiner[1,6] · J. W. Fowler[4] · J. D. Gard[4] · G. C. Hilton[4] · R. L. Kelley[1] · C. A. Kilbourne[1] · J. A. B. Mates[4] · A. R. Miniussi[1,3] · S. H. Moseley[1] · O. Noroozian[1,7,8] · F. S. Porter[1] · C. D. Reintsema[4] · J. E. Sadleir[1] · K. Sakai[1,3] · S. J. Smith[1,3] · T. R. Stevenson[1] · D. S. Swetz[4] · J. N. Ullom[4] · L. R. Vale[4] · N. A. Wakeham[1,2] · E. J. Wassell[1,5] · E. J. Wollack[1]

Received: 9 November 2017 / Accepted: 7 April 2018 / Published online: 20 April 2018

Abstract We performed small-scale demonstrations at GSFC of high-resolution X-ray TES microcalorimeters read out using a microwave SQUID multiplexer. This work is part of our effort to develop detector and readout technologies for future space-based X-ray instruments such as the microcalorimeter spectrometer envisaged for *Lynx*, a large mission concept under development for the Astro 2020 Decadal Survey. In this paper we describe our experiment, including details of a recently designed, microwave-optimized low-temperature setup that is thermally anchored to the 55 mK stage of our laboratory ADR. Using a ROACH2 FPGA at room temperature, we read out pixels of a GSFC-built detector array via a NIST-built multiplexer chip with Nb coplanar waveguide resonators coupled to rf-SQUIDs. The resonators are spaced 6 MHz apart (at $\sim$ 5.9 GHz) and have quality factors of $\sim$ 15,000. In our

✉ W. Yoon
Wonsik.Yoon@nasa.gov

1 NASA Goddard Space Flight Center, Greenbelt, MD 20771, USA

2 NASA Postdoctoral Program, Universities Space Research Association, Greenbelt, MD 20771, USA

3 University of Maryland, Baltimore County, MD 21250, USA

4 National Institute of Standards and Technology, Boulder, CO 80305, USA

5 SGT Inc., Greenbelt, MD 20706, USA

6 Wyle Information System, McLean, VA 22102, USA

7 National Radio Astronomy Observatory, Charlottesville, VA 22903, USA

8 University of Virginia, Charlottesville, VA 22903, USA

initial demonstration, we used flux-ramp modulation frequencies of 125 kHz to read out 5 pixels simultaneously and achieved spectral resolutions of 2.8–3.1 eV FWHM at 5.9 keV. Our subsequent work is ongoing: to-date we have achieved a median spectral resolution of 3.4 eV FWHM at 5.9 keV while reading out 28 pixels simultaneously with flux-ramp frequencies of 160 kHz. We present the measured system-level noise and maximum slew rates and briefly describe our future development work.

Keywords Microwave multiplexing · Flux ramp · Transition-edge sensor · X-ray spectrometer · Microcalorimeter

1 Introduction

The *Lynx* mission concept [1] is one of four large space missions being studied for the upcoming Astrophysics Decadal Review. It aims to be a true follow-on to the Chandra X-ray Observatory, retaining the exquisite $< 1''$ angular resolution in the soft X-ray band (0.1–12 keV) but with a much larger collecting area and improved instrumentation, including the *Lynx* X-ray Microcalorimeter (LXM), a high-resolution (< 3 eV FWHM) imaging spectrometer. This combination will enable observations essential to understanding the earliest galaxies and supermassive black holes, as well as galaxy formation and the assembly of large-scale structure from the earliest epochs.

As is the case for many next-generation cryogenic instruments, the required sensor technology is in hand to provide the desired performance for LXM, but development is required to build and read out large arrays. For *Lynx* we require a hundred times the number of pixels compared to our state-of-the-art microcalorimeter arrays: a hundred kilopixels are needed to match the spatial resolution of the *Lynx* optic while covering a central $5' \times 5'$, and an additional 50 kilopixels are required for an outer array that extends the field-of-view to $20'$ for studies of extended sources. For the inner array we plan to combine thermal and electrical multiplexing techniques by building an array of 'Hydra' microcalorimeters [2], where each sensor is connected to $\sim$25 absorbers, that are read out using microwave SQUID multiplexers (μMUX) [3,4]; the outer array will use standard pixels (1 absorber per sensor) read out using μMUX or a combination of μMUX and code-division multiplexing (CDM) [5,6]. The detector technologies under consideration for LXM are transition-edge sensor (TES) microcalorimeters and metallic magnetic calorimeters (MMCs) [7].

The LXM working group[1] is pursuing several aspects of the instrument development in parallel, including building prototype detector arrays, scalable mulitplexers with appropriate noise and slew-rate requirements, and space-worthy room-temperature readout electronics. In this paper, we highlight our recently developed platform at GSFC intended for small-scale demonstrations of high-resolution X-ray TES microcalorimeters read out via μMUX, and our initial measurement results. Our goals are to demonstrate 32-sensor microwave multiplexing with minimal performance degradation compared to non-multiplexed readout, starting with standard TES

[1] https://wwwastro.msfc.nasa.gov/xrs/SWGs/IWG.html.

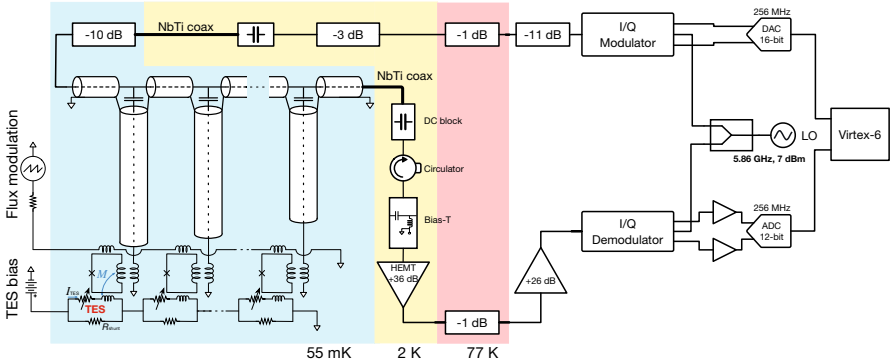

Fig. 1 Circuit diagram of GSFC testbed for high-resolution X-ray microcalorimeter readout demonstrations using microwave SQUID multiplexing. The components on the right (white background) are external to the dewar (Color figure online)

microcalorimeters and moving to Hydra devices suitable for *Lynx*. The latter will demonstrate ∼800 pixels read out using a single 32-channel μMUX chip.

Here we report promising results from our experiments to-date, where we first demonstrated microwave multiplexed read out of 5 pixels, achieving excellent spectral resolution matching that obtained with conventional readout techniques. We have since moved to tests of 32-pixel multiplexing. This latter work is ongoing and, while we present initial results here, we cannot yet present a full description of our system-level performance and limitations, including tradeoffs between various operating parameters, noise levels, and slew-rate capability.

2 Experimental Setup

We retrofitted one of our laboratory dewars typically used for prototype TES testing with components needed for microwave readout of TESs. The dewar uses a LN_2 jacket, a sub-atmospheric LHe bath and an adiabatic demagnetization refrigerator (ADR). Figure 1 presents the circuit diagram and Figs. 2 and 3 show a photograph of the cold-stage (55 mK) plate and sample box.

The μMUX chips contain 33 quarter-wavelength Nb CPW resonators; one end of each resonator is capacitively coupled to a microwave transmission line and the other is inductively coupled to an rf-SQUID. Each resonator has a slightly different length and therefore different resonance frequency. The μMUX, detector, and Nyquist chips are wirebonded together as shown in Fig. 3 so that each TES microcalorimeter circuit is inductively coupled to one rf-SQUID. The TESs are voltage biased using a DC signal that is adjusted to joule heat the TES into its superconducting-to-normal phase transition. An X-ray photon incident on a detector pixel causes a pulsed decrease in the current flowing through the TES, I_{TES}. This produces a change in the SQUID inductance and consequently a shift in the microwave resonance frequency. We apply a sawtooth wave to the flux modulation line, with a peak-to-peak amplitude tuned to produce a change of $\sim 2{-}3\Phi_0$ by the rf-SQUID and frequency of $f_{\mathrm{FR}} \sim 100{-}160$ kHz.

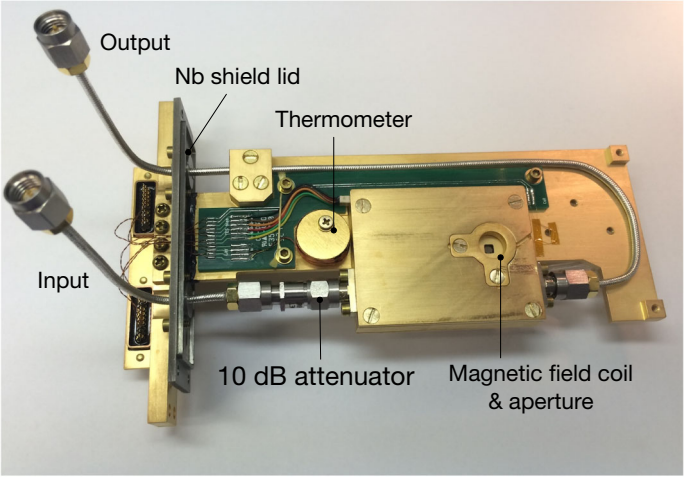

Fig. 2 Photograph of the testing setup. This plate holds the sample box and thermometry. It is inserted into a narrow Nb magnetic shield and thermally anchored to the ADR cold stage. The 2×2 mm^2 aperture on the sample box lid matches the size of our TES array to allow incident X-rays. A superconducting coil is mounted above the TES array to adjust the field environment of the TESs—the coil mounting structure is visible in the photograph (Color figure online)

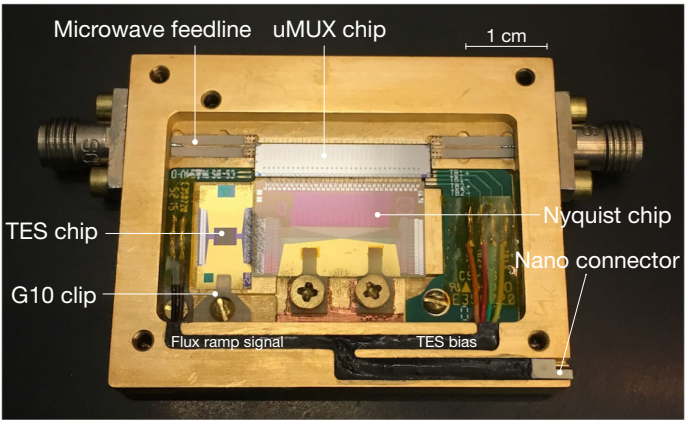

Fig. 3 Sample box without lid. It contains a microwave SQUID multiplexer chip, a TES microcalorimeter array, and a Nyquist chip with inductors and resistors for the TES bias circuit. A 6-pin nanoconnector is used to supply a DC bias to the TESs and the flux-ramp signal for the SQUIDs. The connector cables are fixed with Stycast epoxy in a sidewall pocket (Color figure online)

This flux-ramp modulation [8,9] acts to both linearize the rf-SQUID response and to avoid the well-known $1/f$ noise due to two-level systems in these microwave resonators. With the addition of the flux-ramp modulation, an X-ray signal appears as a phase shift in the SQUID V-Φ, and f_{FR} is the Nyquist sampling rate.

The room-temperature readout system is based on the second-generation of Reconfigurable Open Architecture Computing Hardware platform (ROACH2). A DAC generates a comb of 32 tones from $\sim$ 10 to 128 MHz. These tones are mixed with the

$\sim$ 5–6 GHz LO using an IQ mixer and sent to the μMUX chip to drive the resonators. The transmitted signal is amplified by a low-noise high-electron-mobility transistor (HEMT[2]) at 2 K and again at room temperature, where the signals are then downconverted to the MHz band using an IQ mixer and digitized using an ADC. The ROACH FPGA firmware channelizes the signals from the ADC and demodulates the flux ramp. The resulting data are sent via ethernet to our data acquisition system. Further details about the room-temperature electronics configuration and heritage may be found in Ref. [4].

Figures 2 and 3 show details of the design of the cold-stage components for the μMUX demonstration. During initial cooling, a mu-metal shield is used to reduce the magnetic field trapped by a superconducting Nb shield attached to the ADR cold stage. When the Nb temperature is less than 9 K, the Nb box becomes the main magnetic shield. The 9×50 mm^2 insertion area of this narrow Nb magnetic shield (not pictured) was the most stringent mechanical constraint on the design. The subsequent design of the Cu sample box resulted in an inner volume of $41 \times 24 \times 3.3$ mm^3. We calculated that the cavity resonance frequency of the sample box is approximately 7 GHz, sufficiently high given the aim to operate μMUX chips with resonator frequencies of 5–6 GHz.

We performed multiplexing tests with two separate 8×8-pixel TES microcalorimeter arrays. The array selected for our first tests had the advantage that it has a 'standard' GSFC pixel design and has been well studied over the past decade [10], but the disadvantage that the wiring layout allows only 16 pixels to be coupled to the 32-channel multiplexer chip. Conversely, the second array, pictured in Fig. 3, has a TES pixel design that has not been thoroughly studied, but does have wiring compatible with the 32-pixel multiplexer. For tests with this second array, half of the pixels were coupled to the μMUX chip and the other half were not coupled. In Fig. 3 it is the right half of the TES pixels that are bonded to the Nyquist chip.

In both detector arrays, the TESs are Mo/Au bilayers with three noise-mitigating Au stripes. Each TES sits on a SiN membrane to control the conductance to the thermal bath and has a 240×240 μm^2 overhanging Au/Bi X-ray absorber. Reference [11] presents fabrication details of the GSFC TES arrays. For the first array, the TESs are 140×140 μm^2 squares and the absorber-contact stem area is 'T'-shaped. The devices have T_c of 95 mK, heat capacity of $C \sim 0.86$ pJ/K at T_c, and showed relatively uniform performance of 3 eV FWHM at 5.9 keV on 16 pixels [10]. For the second array, the TESs are 120×120 μm^2 squares and the absorber is attached to each TES through two posts, with four additional posts that mechanically support the absorber but do not electrically connect to the TES. Based on representative devices measured on a similar chip, we expect T_c of 91 mK and heat capacity of $C \sim 1.1$ pJ/K at T_c. With a conventional single-channel DC SQUID readout using a flux-locked loop we measured 2 pixels from this representative chip and obtained spectral performance of $\Delta E_{\mathrm{FWHM}} = 2.6 \pm 0.1$ eV and 3.5 ± 0.1 eV at 5.9 keV, significantly broader than the 2.1 eV predicted for each pixel based on the measured signal size and noise. The Nyquist chip has shunt resistors with $R_s = 0.2$ mΩ and Nyquist inductors of

[2] We use a HEMT from Low-Noise Factory (Model LNF-LNC4_8C) that has a noise temperature of 2.3 K.

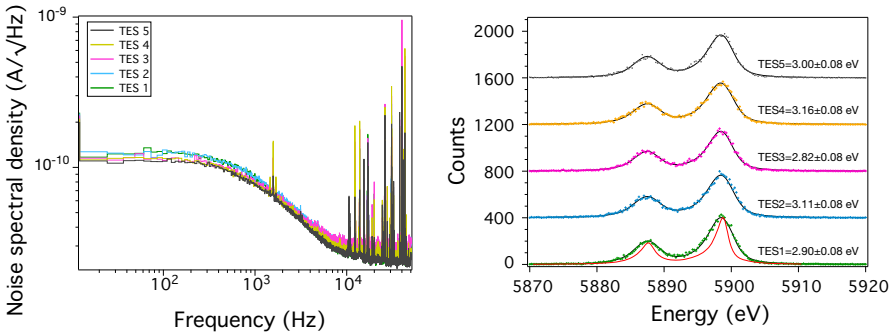

Fig. 4 Left: noise spectral density of five TES detectors read out using microwave SQUID multiplexed readout. Right: Mn Kα spectra for the five pixels. The incident X-ray flux was $\sim$ 1.5 ct/s/pixel (Color figure online)

$L_N = 200$ nH, the latter designed to slow the pulse rise time and thus relax the slew-rate requirement on the readout.

The microwave SQUID multiplexing chip was fabricated by NIST. The 33 resonators are designed to have resonance frequencies of $\sim$ 5.7–6.0 GHz and bandwidths of 300 kHz. The resonators are grouped into two bands: resonators within each band are separated by 6 MHz and there is a 20 MHz gap between the two bands. Of the 33 resonators, one has a 'dark' SQUID that does not connect to a TES. The other 32 resonators are coupled to TES detectors. The measured resonator quality factors are $Q \sim$13,500 ($Q_c \sim$ 14,500, $Q_i \sim 1.5 - 2 \times 10^5$).

3 Measurement Results

For our initial demonstration, we set the LO frequency at 5.75 GHz, lower than all of the resonator center frequencies. The microwave drive power at the chip was ~ -70 dBm and the flux-ramp signal was a $f_{FR} = 125$ kHz sawtooth wave with peak-to-peak amplitude of 255 μA, tuned to produce $\sim 3\Phi_0$ per flux-ramp period; we used 2 of the $3\Phi_0$ to demodulate the signal. The bath temperature was 55 mK $\pm$ 1 μK and a common TES bias of 500 μA was applied to bias the TESs at $R/R_n \sim 15\%$.

The results of this demonstration using the first TES array (see Sect. 2) were very promising and are summarized in Fig. 4. The μMUX system was able to track the fast rise of the individual X-ray pulses, and we achieved spectral resolutions of 2.8–3.1 eV FWHM on 5 pixels, which are not significantly degraded compared to the expected energy resolution of $\sim$ 2.8 eV based on signal and noise measurements as well as those obtained using conventional SQUID readout [10]. The noise floor was 30 pA/$\sqrt{\text{Hz}}$ and the maximum slew rate was 0.33 A/s. The data in Fig. 4 were acquired while driving 5 resonators only; however, we measured nearly identical noise on those 5 channels while driving 16 resonators spaced 6 MHz apart (5 coupled to TESs, 11 without TESs), suggesting that we would achieve similar spectral resolution for at least 16-pixel multiplexed readout.

For our subsequent demonstration, we used the second TES array, which has a wiring layout that enables 32 detector pixels to be coupled to the 32 available resonators

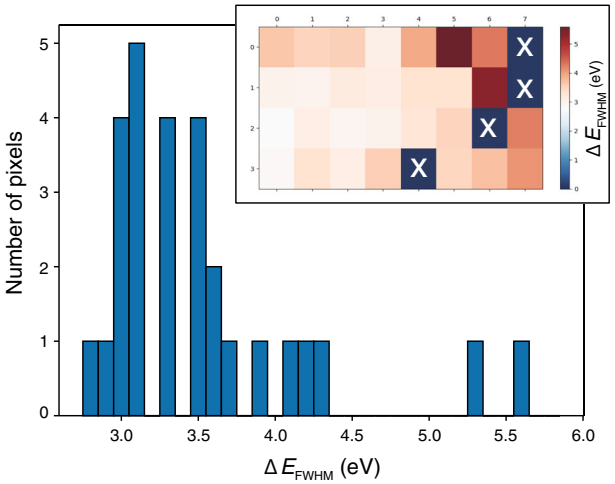

Fig. 5 Histogram of spectral resolution at 5.9 keV of the 28 TES microcalorimeters measured using microwave SQUID multiplexed readout. The energy resolution distribution was $\Delta E_{\mathrm{FWHM}} = 2.8 - 4.3$ eV with two outliers at 5.3 and 5.6 eV owing to high detector noise. The upper right panel presents a 2D map of the TES position with energy resolution. The 4 pixels not measured are marked with an "X" (see text). The half of this 64-pixel array that was not biased would appear at the top of the plot. The incident X-ray flux was $\sim$ 1.5 ct/s/pixel (Color figure online)

on the μMUX chip (see Sect. 2). For this demonstration, a LO frequency of 5.86 GHz was chosen to reside in the 20 MHz gap between the two bands of resonators and the microwave drive power at the chip was ~ -70 dBm. The flux-ramp signal was a $f_{\mathrm{FR}} = 160$ kHz sawtooth wave with peak-to-peak amplitude of 189 μA, tuned to produce $\sim 2\Phi_0$ per flux-ramp period; we used 1 of the $2\Phi_0$ for demodulation. The bath temperature was 55 mK and a common TES bias of 410 μA was applied to bias the TESs at $R/R_{\mathrm{n}} \sim 20\%$; this bias current was calculated based on IV measurements of the representative devices as we did not have a process in place to measure TES IV curves using the microwave system.

We read out 31 resonators simultaneously while illuminating the array with MnKα photons from an ^{55}Fe source external to the dewar. Figure 5 provides a histogram of the resulting spectral resolution measurements of 28 pixels. The median resolution was 3.35 eV FWHM and, excluding the two outliers at > 5 eV, the average measured resolution was 3.4 eV while the average expected resolution based on signal and noise measurements was 3.2 eV. The increase in f_{FR} and decrease from $3\Phi_0$ to $2\Phi_0$ per flux-ramp period were chosen to allow operation at higher slew rates. We measured a maximum slew rate of 0.60 A/s, twice that achieved in the first demonstration.

Three channels showed no response to TES signals due to the damage of Nyquist inductors or incorrect wiring and thus were not measured in the demonstration, but the corresponding three resonators were driven. A fourth resonator was not used to avoid interference with a nearby resonator. The inset of Fig. 5 shows the energy resolution of each TES pixel as a function of position in the array. The map shows a gradient in energy resolution, with the best pixels near the lower left corner. There is a similar gradient in the signal size and in predicted energy resolution based on signal and noise:

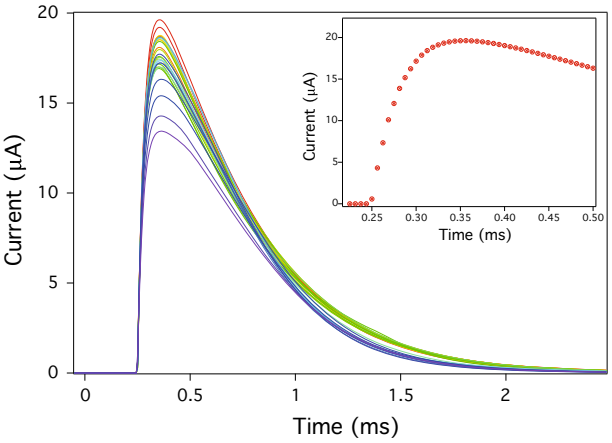

Fig. 6 Pulse heights of the 28 TES microcalorimeters measured using microwave SQUID multiplexed readout. The gradient in signal size was not expected and was likely due to a gradient in heat-sink temperature across the array that caused a difference in TES bias point and a corresponding difference in signal height. Inset: individual data points on the pulse rise highlight the measured maximum slew rate of 0.60 A/s (Color figure online)

Fig. 6 shows the measured pulse height of each pixel, where the smaller pulses tend to be the pixels with worse spectral performance. The gradient in signal size is likely due to a gradient in heat-sink temperature across the array.[3] The two outliers in Fig. 5 with $\Delta E_{\mathrm{FWHM}} > 5$ eV appear dark brown in the map and exhibit excess detector noise that is not associated with the multiplexed readout [12]. The readout noise level was $\sim 60\ \mathrm{pA}/\sqrt{\mathrm{Hz}}$, which contributed a significant noise term to this demonstration, rendering the expected energy resolution (for the pixels with the largest pulse height) ~ 2.8 eV as compared to 2.1 eV for similar pixels measured with our conventional DC SQUID single-channel readout. This noise floor was higher than the $30\ \mathrm{pA}/\sqrt{\mathrm{Hz}}$ level measured in our first demonstration and $19\ \mathrm{pA}/\sqrt{\mathrm{Hz}}$ that was achieved with a similar μMUX chip in Ref. [4]. Investigations of this noise floor are ongoing, but likely are related to our choice of flux-ramp modulation/demodulation parameters and resonator drive power, not a fundamental limitation.

4 Summary and Conclusions

We presented the first results using a microwave SQUID multiplexer to read out an array of high-resolution X-ray microcalorimeters. This work is part of our program to increase the technology readiness level of the detector system for *Lynx*. We simul-

[3] We posit that a temperature gradient across the array was established due to particle debris causing heating on the nearby MUX chip. The pixels closest to the MUX chip showed the smallest pulse heights (consistent with an elevated heat-sink temperature) whereas the pixels farthest from the MUX chip showed pulse heights similar to those expected for a heat-sink temperature of 55 mK. Following this experiment, debris was identified on the MUX chip and removed; the pulse-height gradient was not observed on prior or subsequent tests.

taneously obtained spectra from 5 pixels with an average of 3.0 eV FWHM energy resolution at 5.9 keV with no degradation compared to conventional readout and, as part of our ongoing work, read out 28 pixels with a median energy resolution of 3.35 eV FWHM at 5.9 keV and a maximum slew rate of 0.60 A/s. These initial demonstrations are very promising, and our future work will focus on understanding and optimizing the system-level performance.

References

1. J.A. Gaskin et al., Proc. SPIE **10397**, 103970S (2017). https://doi.org/10.1117/12.2273911
2. S.J. Smith, S.R. Bandler, R.P. Brekosky, A.-D. Brown, J.A. Chervenak, M.E. Eckart, E.F.-Feliciano, F.M. Finkbeiner, R.L. Kelley, C. A. Kilbourne, F.S. Porter, J.E. Sadleir, IEEE Trans. Appl. Supercond. **19** (2009). https://doi.org/10.1109/TASC.2009.2019557
3. J.A.B. Mates, G.C. Hilton, K.D. Irwin, L.R. Vale, K.W. Lehnert, Appl. Phys. Lett. **92** (2008). https://doi.org/10.1063/1.2803852
4. J.A.B. Mates, D.T. Becker, D.A. Bennett, B.J. Dober, J.D. Gard, J.P. Hays-Wehle, J.W. Fowler, G.C. Hilton, C.D. Reintsema, D.R. Schmidt, D.S. Swetz, L.R. Vale, J.N. Ullom, Appl. Phys. Lett. **111** (2017). https://doi.org/10.1063/1.4986222
5. C.D. Reintsema, J. Beall, W. Doriese, W. Duncan, L. Ferreira, G.C. Hilton, K.D. Irwin, D. Schmidt, J. Ullom, L. Vale, Y. Xu, J. Low Temp. Phys. **151**, 927–933 (2007). https://doi.org/10.1007/s10909-008-9769-7
6. K.M. Morgan, B.K. Alpert, D.A. Bennett, E.V. Denison, W.B. Doriese, J.W. Fowler, J.D. Gard, G.C. Hilton, K.D. Irwin, Y.I. Joe, G.C. O'Neil, C.D. Reintsema, D.R. Schmidt, J.N. Ullom, D.S. Swetz, Appl. Phys. Lett. **109** (2016). https://doi.org/10.1063/1.4962636
7. A. Fleischmann, C. Enss, G.M. Seidel, Metallic magnetic calorimeters, in cryogenic particle detection, *Topics in Applied Physics*, ed. by C. Enss, vol. 99, pp. 151–216 (2005)
8. J.A.B. Mates, K.D. Irwin, L.R. Vale, G.C. Hilton, J. Gao, K.W. Lehnert, J. Low Temp. Phys. **167** (2012). https://doi.org/10.1007/s10909-012-0518-6
9. O. Noroozian, J.A.B. Mates, D.A. Bennett, J.A. Brevik, J.W. Fowler, J. Gao, G.C. Hilton, R.D. Horansky, K.D. Irwin, Z. Kang, D.R. Schmidt, L.R. Vale, J.N. Ullom, Appl. Phys. Lett. **103** (2013). https://doi.org/10.1063/1.4829156
10. C.A. Kilbourne, W.B. Doriese, S.R. Bandler, R.P. Brekosky, A.-D. Brown, J.A. Chervenak, M.E. Eckart, F.M. Finkbeiner, G.C. Hilton, K.D. Irwin, N. Iyomoto, R.L. Kelley, F.S. Porter, C.D. Reintsema, S.J. Smith, J.N. Ullom, Proc. SPIE **7011**, 701104–701107 (2008)
11. E.J. Wassell et al., IEEE Trans. Appl. Supercond. **27**(4) (2017). https://doi.org/10.1109/TASC.2016.2633783
12. S.J. Smith, J.S. Adams, C.N. Bailey, S.R. Bandler, S.E. Busch, J.A. Chervenak, M.E. Eckart, F.M. Finkbeiner, C.A. Kilbourne, R.L. Kelley, S.-J. Lee, J.-P. Porst, F.S. Porter, J.E. Sadleir, J. Appl. Phys. **114** (2013). https://doi.org/10.1063/1.4818917